

VORTEX BEHAVIORS OVER A CRANKED ARROW WING CONFIGURATION AT HIGH ANGLES OF ATTACK

Dong-Youn KWAK*, Masashi SHIROTAKE** and Kenichi RINOIE**

*Japan Aerospace Exploration Agency, Tokyo, 181-0015, JAPAN,

**Department of Aeronautics and Astronautics, University of Tokyo, 113-8656, JAPAN

Keywords: SST, Leading-edge separation vortex, Vortex interaction

Abstract

Wind tunnel tests were performed to investigate the vortex behaviors over a cranked arrow wing configuration with leading-edge flaps at high angles of attack. Vortical flows of the leeward wing were surveyed by the stereoscopic PIV and the oil flow techniques. Static pressure measurements were performed at the Reynolds number of 9.21×10^5 based on the wing root chord. The flow fields over the cranked arrow wing were investigated when the inboard vortex flaps and outboard leading-edge flaps were deflected separately. Interactions between inboard and outboard vortices are observed downstream of the wing kink position. These vortex interactions induce the change of the vertical vortex position and the chordwise location of the vortex breakdown both for the inboard and outboard vortices

Nomenclature

b	local span length, m
b_{\max}	wing maximum span length, m
C_{mac}	wing mean aerodynamic chord length, m
C_p	pressure coefficient
C_r	wing root chord length at model center-line, m
Re	Reynolds number based on mean aerodynamic chord
U_∞	free stream velocity, m/s
u	mean velocity in x direction, m/s
v	mean velocity in y direction, m/s
w	mean velocity in z direction, m/s

x	chordwise coordinate measured from apex of the cranked arrow wing at model center line, m
y	spanwise coordinate measured orthogonal to x from model center line, m
z	coordinate orthogonal to x and y measured from model center-line, m
Λ	sweep back angle, degree
α	angle of attack, degree
$\delta_{f\text{LE-in}}$	inboard leading-edge vortex flap deflection angle, degree
$\delta_{f\text{LE-out}}$	outboard leading-edge flap deflection angle, degree
ω	x -direction vorticity in y - z plane, 1/sec

1 Introduction

Higher sweepback angle and lower aspect ratio wing is adopted as the main wing of a high-speed aircraft such as a Supersonic Transport (SST). When compared to a delta wing, a double delta wing and cranked arrow wing planforms indicate higher aerodynamic performance and maneuverability at high angles of attack, because a vortex generated from the strake wing (or the inboard wing) stabilizes the flow on the main wing (or the outboard wing), and because the vortex generates so called vortex lift [1]. Furthermore, the outboard wing leading-edge that has smaller sweepback angle than that of the inboard wing increases the wing aspect ratio as a whole and low-speed performance is improved. When the wing angle of attack is increased further, nonlinear vortex behaviors such as a vortex breakdown and a

vortex lift-off occur abruptly and they change the aerodynamic characteristics of these wings.

A number of researches on the double delta wing configurations have been made since 1970's [2-7]. Fiddes and Smith [2] reported that the strake (inboard) vortex induces the upwash and the sidewash near the kink of the inboard and outboard leading-edge, and that the formation of the outboard leading-edge vortex is promoted. Olsen and Nelson [3] concluded that the breakdown of the outboard vortex is delayed because lateral velocity caused by the strake vortex supplies the kinematic energy to the outboard vortex. Thompson [4] and Brennenstuhl et al [5] performed wind tunnel tests on a series of double delta wing. They investigated the vortex interactions between the inboard and outboard vortices when the sweepback angles of the outboard leading-edge were changed. Verhaagen et al [6,7] reported that the breakdown of the main wing vortex is triggered by the breakdown of the strake vortex when these vortices interacted with each other. These researches indicated that the vortex interactions on the double delta wing are highly dependent on the angles of attack and the inboard and the outboard sweepback angles.

Most of these researches were performed only for typical double delta wing configurations that have higher sweepback angle on the inboard leading-edge ($\Lambda_{in}=80^\circ$ or 76°). They are focused mainly on the outboard vortex behaviors because inboard wings were designed using the concept of the strake wing and because the inboard wing has relatively small wing area. On the other hand, cranked arrow wing has usually smaller inboard sweepback angle and wider inboard wing area when compared to the double delta wing tested in Refs. [2-7]. However, there are only a few references that investigated the vortex interactions on a cranked arrow wing. The effect of the vortex interactions on the cranked arrow wing performance has not been clarified yet.

In the present research, wind tunnel tests were performed to investigate the vortex behaviors on a cranked arrow wing that has relatively small inboard leading-edge

sweepback angle ($\Lambda_{in}=66^\circ$) (outboard sweepback angle is 42°). Vortical flows on the leeward wing were measured by the stereoscopic Particle Image Velocimetry (PIV) technique and observed by the oil flow technique. Static pressure measurements were also conducted. Interactions between the inboard and the outboard vortices were investigated when the strengths of each inboard and outboard vortices are altered by means of the inboard leading-edge vortex flaps and the outboard leading-edge flaps.

2 Experimental Details

Wind tunnel tests were conducted in a $2\text{m} \times 2\text{m}$ low speed wind tunnel at Japan Aerospace Exploration Agency (JAXA). A free-stream velocity was $U_\infty=30\text{m/s}$ and the Reynolds number based on the mean aerodynamic chord was $Re=9.21 \times 10^5$.

Figure 1 shows an SST model that is preliminarily designed in the supersonic transport program of JAXA [8]. This SST configuration model consists of a cranked arrow wing and a fuselage. The kink point is located at $y/(b_{max}/2)=0.55$ that connects the inboard wing with 66° sweep back angle and the outboard wing with 42° sweep back angle. The wing is designed by the supersonic lifting surface theory to optimize the twist and camber distributions at a design Mach number of 1.7 [8]. The leading edge of this model was modified so that it has the vortex flaps [9] on the inboard wing and the leading edge flaps on the outboard wing. The leading-edge vortex flap is effective when it is used for a highly swept-back delta wing such as the inboard wing of the present model. The tested deflection angles of the inboard leading edge vortex flap are $\delta_{f\text{LE-in}}=0^\circ$ and 30° which are defined as the angle measured in the plane that is normal to the hinge line (see figure 1). The outboard flap deflection angles are $\delta_{f\text{LE-out}}=0^\circ$ and 12.2° which are defined as the angle measured parallel to the free stream. In the present research, wind tunnel test was performed for the following three models. 1) The baseline configuration that has no flap deflection ($\delta_{f\text{LE-}}$

$\delta_{f\text{LE-in}}=0^\circ$, $\delta_{f\text{LE-out}}=0^\circ$), 2) the model when only the inboard flaps are deflected 30° ($\delta_{f\text{LE-in}}=30^\circ$, $\delta_{f\text{LE-out}}=0^\circ$), 3) the model when only the outboard flaps are deflected 12.2° ($\delta_{f\text{LE-in}}=0^\circ$, $\delta_{f\text{LE-out}}=12.2^\circ$). The SST model has static pressure tappings on the upper surface of the left wing at $x/C_r=0.55$ and 0.83 as shown in figure 1. The inboard wing has a thickness distribution of a NACA66-series airfoil. The outboard wing has a biconvex airfoil section with a maximum thickness chord ratio of 3%. Further details of the wing cross section are described in references [9-11].

A schematic of wind tunnel tests is shown in figure 2. The SST model was supported by an industrial multi-purpose robot-arm via the sting. The robot-arm can control the model attitude with six-degrees of freedom within 0.2mm accuracy [12]. The tested angles of attack were 8° , 12° , 16° and 20° .

Electronic scanning pressure sensors are used to measure the surface static pressure. Static pressure data were obtained by averaging 100 sample a data recorded in 5msec interval. The repeatability of pressure coefficients was within $\Delta C_p=0.03$.

Stereoscopic PIV surveys were performed to understand the overall behaviors of flows at different chordwise locations. The PIV system (figure 2) mainly consists of 200mJ double-pulse Nd:YAG lasers to illuminate the seeding particles in the flow, two CCD cameras with 1280×1048 pixels to acquire images of the illuminated particles, and a PC to control the equipments and to conduct data processing. Detail information on the present PIV system is described in reference [13]. Oil droplets of an approximate average diameter of $1\mu\text{m}$ were inserted into the flow as seeding particles. The laser light sheet introduced through an upper optical window of the test section illuminates the seeding particles over the upper surface of the model. This sheet is parallel to the y-z crossflow plane based on the model body axis. Two CCD cameras were located at the port side of the wind tunnel test section. Each camera with $30\mu\text{sec}$ time interval acquired instantaneous two particle images. Three

component velocities (u , v , w based on the body axis) were calculated from captured images from two CCD cameras. Typical imaging area size was 250mm in width and 80mm in height. Averaged flow velocity vector distributions were obtained by averaging 300-900 sheets of instantaneous velocity vector images with an acquisition rate of 2Hz. The detail data validation on these test are described in reference [13].

Overall surface flow patterns were visualized by means of the oil flow technique.

3 Results and Discussion

3.1 Vortex Behaviors on the Baseline Configuration

In this section, overall flow fields on the baseline configuration ($\delta_{f\text{LE-in}}=0^\circ$, $\delta_{f\text{LE-out}}=0^\circ$) at different angles of attack are summarized.

3.1.1 Oil flow patterns

Figure 3 shows the upper surface oil flow patterns at $\alpha=12^\circ$ and 20° . Two vortical flow patterns, reattachment lines and secondary separation lines are observed clearly at $\alpha=12^\circ$. Both vortical flow patterns grow conically as the chordwise location moves to downstream.

A spanwise distance between the inboard reattachment line and the secondary separation line (the width of the inboard vortical flow pattern) at upstream of the kink increases as the angle of attack is increased from $\alpha=12^\circ$ to 20° . These results correspond to the vortex grow up with increasing the angle of attack. Vortical flow pattern of the outboard wing are dismissed near $x/C_r=0.85$ downstream of the kink position. At the same time, secondary separation line of the outboard vortex is curved abruptly toward the wing tip. Thus, the inboard flow pattern can only be observed downstream of $x/C_r = 0.85$. It is suggested that flows downstream of $x/C_r = 0.85$ are mainly dominated by the inboard vortex.

3.1.2 Vortical flow fields

Figure 4 shows average velocity vectors and streamwise velocity contour at different chordwise locations at $\alpha=12^\circ$. The inboard and outboard vortices originate from the inboard and

outboard leading-edges (figure 3). At $x/C_r = 0.83$, an area in which the streamwise velocity decreases at the center of inboard vortex is revealed. Further decrease in the streamwise velocity at the center of inboard vortex are observed at $x/C_r = 0.98$. We can suggest that the vortex breakdown [14] is occurred at this chordwise station. The vortex breakdown is hereafter defined as the state when the x -direction velocity u is nearly 0. On the other hand, concentrated strong vortex is formed on the outboard wing at $x/C_r = 0.83$. While the streamwise velocity at the outboard vortex center decreases abruptly at $x/C_r = 0.98$.

Figure 5 shows average velocity vectors and streamwise velocity contours at different chordwise locations at $\alpha = 20^\circ$. When compared to those at $x/C_r = 0.4, 0.55, \alpha = 12^\circ$ in fig.4, cross flow velocity components at the same chordwise station is faster than those at $\alpha = 12^\circ$ in general. Streamwise velocities are also faster than those at $\alpha = 12^\circ$. The strength of the inboard vortex is increased and grown up as the angle of attack is increased up to $\alpha = 20^\circ$. However abrupt decrease in the streamwise velocity at the center of inboard vortex downstream of $x/C_r = 0.7$ is observed that indicates the vortex has broken down at around this chordwise station. At $\alpha = 20^\circ$, the chordwise location of the vortex breakdown is moved upstream when compared to that at $\alpha = 12^\circ$. However, the concentrated vortex is seen on the outboard wing that has not been broken down at $x/C_r = 0.83$. The position of the outboard vortex is located further away from the model surface when compared to that at $\alpha = 12^\circ$. At $x/C_r = 0.98$, the outboard vortex that has been broken down is located far away from the surface, and at the same time, the inboard vortex moves toward downward position. These changes of the vortex positions at $\alpha = 20^\circ$ are caused by the mutual vortex interactions. The induced velocity of the inboard and outboard vortices affects each other and then both vortices change their positions. These behaviors of the vortices could be corresponded to the oil flow patterns seen in figure 3; i.e. the flow pattern of the outboard vortex is dismissed from the surface and the secondary separation line of the inboard

vortex abruptly curves toward the wingtip at $x/C_r = 0.85$. Though the merging of the inboard and outboard vortices was not observed in the present tests, it can be clarified that the inboard and outboard vortices interact with each other.

Figure 6 shows the x -direction vorticity (ω) distribution at different chordwise locations at $\alpha = 20^\circ$. The vorticities are generated from inboard and outboard leading-edges. Since the vorticity is not supplied into the inboard vortex downstream of the kink ($x/C_r = 0.83, 0.98$) from the leading-edge, the strength of the vortex weakens by the viscous effects. The vorticity decreases abruptly when the vortex breakdown occurs.

At $x/C_r = 0.25$, there is an area where high vorticity is observed over the fuselage. That is a body vortex formed from the nose part of the fuselage. Downstream of $x/C_r = 0.25$, the body vortex weakens and it is pulled into the strong inboard vortex. Because the body vortex is very weak when compared to the inboard vortex, there are no obvious effects on the wing aerodynamic characteristics.

3.1.3 Spanwise Pressure Distributions

Spanwise C_p distributions at $x/C_r = 0.55$ and 0.83 are shown in figure 7. As the angle of attack is increased from 8° to 20° , the absolute value of C_p at the suction peak at $x/C_r = 0.55$ is increased. The spanwise location of the suction peak slightly moves into inboard direction. The same tendency was observed for the plain delta wing when the vortex has not been broken down [15]. At $x/C_r = 0.83$, two suction peaks are observed. Each suction peak corresponds to the inboard and outboard vortices. The absolute value of C_p at the inboard suction peak is increased as the angle of attack increases, while the C_p distributions around this suction peak lose their distinctive peak. The breakdown point moves from the trailing-edge to the apex as the angle of attack is increased [15]. When the vortex breaks down, the vortex core is diverged and velocity inside the vortex is decreased that cause the loss of the vortex lift. On the other hand, the absolute value of C_p at the suction peak on the outboard wing at $\alpha = 20^\circ$ is smaller than that at $\alpha = 16^\circ$. When the

angle of attack is increased, the outboard vortex moves to the upward direction due to the vortex interaction with the inboard vortex, so that the absolute value of C_p at the suction peak is decreased. On the contrary, the inboard vortex moves to the downward direction due to the vortex interaction those vortex movement contribute to increase the absolute value of C_p .

3.2 Interaction with Inboard and Outboard Vortices

In this section, we summarize the interactions with the inboard and outboard vortices that are important factor to understand the vortex behaviors on the cranked arrow wing configurations. As mentioned in the Introduction, the inboard leading-edge vortex flap and the outboard leading-edge flaps have strong effects on the strength of the leading edge vortices formed on the wing. For example, the inboard leading edge vortex flap delays the formation and growing up of the inboard vortex when compared to the baseline configuration [10]. Therefore the interaction between inboard and outboard vortices would decrease as the inboard vortex flaps are deflected. The outboard leading-edge flap would also reduce the vortex interactions because this flap restrains the formation of the outboard vortex. When the behavior of the outboard vortex is discussed by comparing the results with and without inboard vortex flap deflections, the effects of the interaction on the outboard vortex can be clarified. The interaction on the inboard vortex can also be clarified when the comparisons are made for the models with and without the outboard leading-edge flap deflections.

3.2.1 Vortex Flow Fields

Figure 8 shows averaged velocity vectors and streamwise velocity contours for the different leading-edge flap deflection angles. When compared to the behaviors of the outboard vortex at $x/C_r = 0.83$ with and without inboard leading edge flap deflections, no breakdown is observed on the baseline configuration (fig.8a and 8d), while the outboard vortex breakdown is

observed on the model of the inboard leading-edge flap deflection (fig.8b and 8e). The vortex interaction on the baseline configuration is stronger than that of the model with the inboard flap deflection, because the vortex interaction delays the breakdown of the outboard vortex [3-5]. These behaviors are caused by 1) the supply of the kinematic energy from lateral velocity that is induced by the inboard vortex. 2) the outboard vortex moves to the upward direction by the induced velocity of the inboard vortex, therefore the viscous effect near the wing surface decreases.

When compared to the behaviors of the inboard vortex with or without the outboard leading edge flap deflection (fig.8c, 8f), the inboard vortex on the model with the outboard flap deflection is located more inboard and upward than that on the baseline configurations. Therefore, a length between the inboard and outboard vortex cores is larger than that on the baseline configurations. It means that vortex interaction becomes weak on the model with the outboard flap deflection. The area where the low streamwise velocity is observed at the inboard vortex on the model when the outboard leading edge flap is deflected is larger than the similar area for the baseline configuration. From these results, it can be suggested that the chordwise position of the inboard vortex breakdown on the model with outboard flap deflection is located more upstream than that of the baseline configuration.

Figure 9 shows the spanwise velocity and total velocity distribution along the $y = -300\text{mm}$ at $x/C_r = 0.83$ for three different wing configurations. Spanwise velocity distributions (v :y-direction velocity component) on the baseline configuration are faster than the model with the outboard flap deflection in general. The spanwise velocity is induced by the outboard vortex that supplies the kinematic energy to the inboard vortex. Hence, the results in fig.9 clarify the above discussion that the inboard vortex is stabilized due to the induced velocity of the outboard vortex and therefore the inboard vortex breakdown position is located downstream for the wing with outboard flap deflection.

3.2.2 Spanwise Pressure Distributions

Spanwise C_p distributions at $x/Cr=0.55$ and 0.83 are shown in Figure 10. At $x/Cr=0.55$, $\alpha=12^\circ$ (fig.10a), the C_p distributions on the baseline configuration are almost identical to those on the outboard flap deflection. This means that the outboard flap does not affect the flow at $x/Cr=0.55$ (upstream of the kink position), $\alpha=12^\circ$. The absolute value of C_p at suction peak on the baseline configuration is higher than that on the model with outboard flap deflections at $\alpha=20^\circ$ (fig.10b). As mentioned in section 3.2.1, the interactions between inboard and outboard vortices on the baseline configuration are stronger than that of the model with the outboard flap deflection. At $x/Cr=0.83$, it was shown in fig.8 that the vertical position of the inboard vortex on the baseline configuration is closer to the wing surface than that of the outboard flap deflection. It is suggested that the effects of the vortex interaction downstream of the kink position can spread into the upstream position ($x/Cr=0.55$) at $\alpha=20^\circ$. This causes the inboard vortex position on the baseline configuration to locate closer to the surface than that of the outboard flap deflection. Therefore the C_p of the baseline configuration has higher suction peaks than that of the model with outboard flap deflection even at $x/Cr=0.55$ upstream of the kink position.

When the C_p distributions of the baseline configuration are compared with those of the model with outboard flap deflection, relatively low suction peak is observed on the inboard wing of the model with outboard flap deflections when compared to that on the baseline configuration (fig.10d). The low suction peak on the inboard wing of the model with outboard flap deflections is induced by the following two factors: 1) the chordwise position of the inboard vortex breakdown is located more upstream than that of the baseline configuration, 2) the vortex center position on the model with the outboard flap deflection is located further away from the surface than that of the baseline configuration (fig.8).

Upper surface pressure distributions are strongly influenced by vortex breakdown behaviors and vortex positions that are induced by inboard and outboard vortex interactions.

4 Conclusions

Wind tunnel tests were performed to investigate the vortex behaviors on a cranked arrow wing configuration at high angles of attack. Interactions between the inboard and outboard vortices were discussed by comparing the results of the models with the inboard and outboard leading edge flap deflections.

- 1) When $\alpha=20^\circ$, three pairs of leading edge separation vortices are formed on the inboard, outboard wing leading edges and on the fuselage. Those vortices are broken down on the wing surface. The inboard vortex breaks down more upstream position than that of the outboard vortex.
- 2) Interactions between inboard and outboard vortices are observed downstream of the kink position. The inboard and outboard vortices influenced with each other by induced velocity. Those vortex interactions cause the inboard vortex to move downward and that of the outboard vortex to move upward, and delay the occurrence of the inboard and outboard vortex breakdown.

References

- [1] Polhamus E C. Predictions of Vortex-Lift Characteristics by a Leading-Edge Suction Analogy, *Journal of Aircraft*, Vol.8, No4, pp193-199, 1971.
- [2] Fiddes S P and Smith J H B. Strake-Induced Separation From the Leading Edges of Wings of Moderate Sweep, AGARD-CP-247, Jan. 1979.
- [3] Olsen P E and Nelson R C. Vortex Interaction Over Double Delta Wings at High Angles of Attack, AIAA-Paper 89-2191-Cp, 1989.
- [4] Thompson D H. A Visualization Study of the Vortex Flow Around Double-Delta Wings, ARL-AERO-R-165, 1985
- [5] Brennenstuhl U and Hummel D. Vortex Formation Over Double-Delta Wings, Proceedings of 13th Congress of the International Council of the Aeronautical Science (ICAS Paper 82-6.6.3), Seattle, USA, Aug. 1982, pp 1302-1309.

VORTEX BEHAVIORS OVER A CRANKED ARROW WING CONFIGURATION AT HIGH ANGLES OF ATTACK

- [6] Verhaagen N G and Maseland J E J. Investigation of the Vortex Flow Over A 76/60-deg Double Delta Wing at 20deg Incidence, AIAA-Paper 91-3208-CP, 1991.
- [7] Verhaagen N G, Jenkins L N, Kern S B and Washburn A E. A Study of the Vortex Flow Over a 76/40-deg Double-Delta Wing, AIAA-Paper 95-0650, 1995.
- [8] Yoshida K and Makino Y and Shimbo Y. An Experimental Study on Unmanned Scaled Supersonic Experimental Airplane, AIAA-Paper 2002-2842, 2002.
- [9] Rinoie K, Miyata K, Kwak D Y and Noguchi M, Studies on Vortex Flaps with Rounded Leading Edges for Supersonic Transport Configuration, *Journal of Aircraft*, to be published. also ICAS 2002 8-7-3, 2002.
- [10] Kwak D Y, Miyata K, Noguchi M and Rinoie K. Experimental Investigations on High Lift Devices for an SST, National Aerospace Laboratory Technical Report, NAL-TR 1450, 2002. (in Japanese)
- [11] Kwak D Y, Miyata K, Noguchi M, Rinoie K and Fujita T. Roll Characteristics of the SST Configuration with LE Flap and TE Flap at High Angles of Attack, AIAA-Paper 2003-3413, Jun. 2003.
- [12] Fujita T, Iwasaki A, Fujieda H, Shigemi M, Nakayasu H and Sagisaka M, Model Support System Using an Industrial Robot in Low-speed Wind Tunnel, National Aerospace Laboratory Technical Memorandum, NAL-TM 666, 1994
- [13] Watanabe S, Kato H, Kwak D Y, Shirotake M and Rinoie K. Stereo PIV Measurements of Leading Edge on a Cranked Arrow Wing, *Measurement Science and Technology*, Vol.15, No.6, pp1079-1089. 2004.
- [14] Wentz W H and Kohlman D L. Vortex Breakdown on Slender Sharped-Edged Wings, *Journal of Aircraft*, Vol.8, No3, pp156-161, 1971
- [15] Zohar Y and Er-El J. Influence of the Aspect Ratio on the Aerodynamics of the Delta Wing at High Angle of Attack, *Journal of Aircraft*, Vol.25, No.3, pp200-205, 1988.

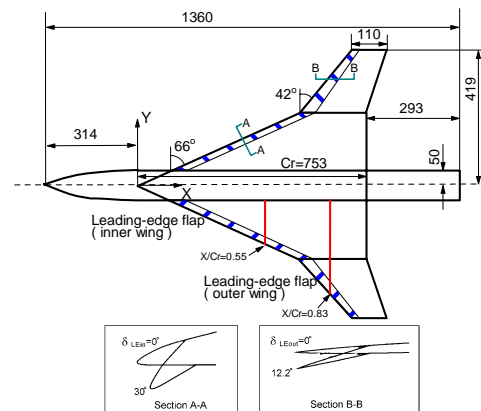


Fig.1 Schematics of the SST model (unit:mm)

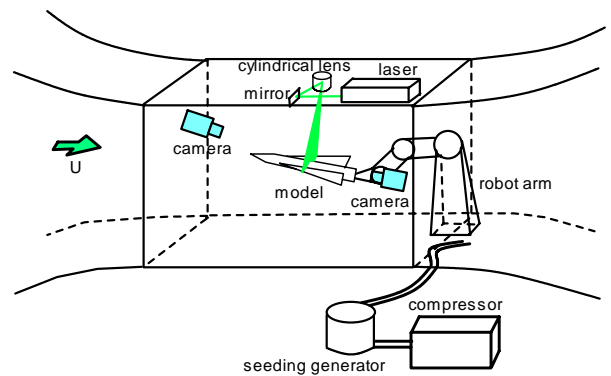
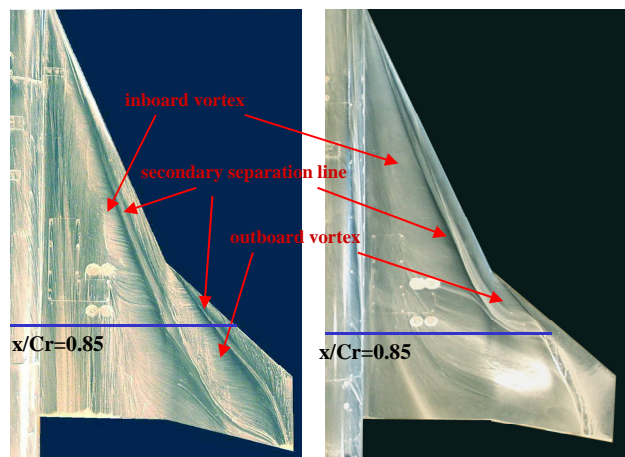


Fig.2 Schematics of experimental set-up (seen from the port side)



(a) $\alpha=12^\circ$

(b) $\alpha=20^\circ$

Fig.3 Oil flow patterns on the upper surface

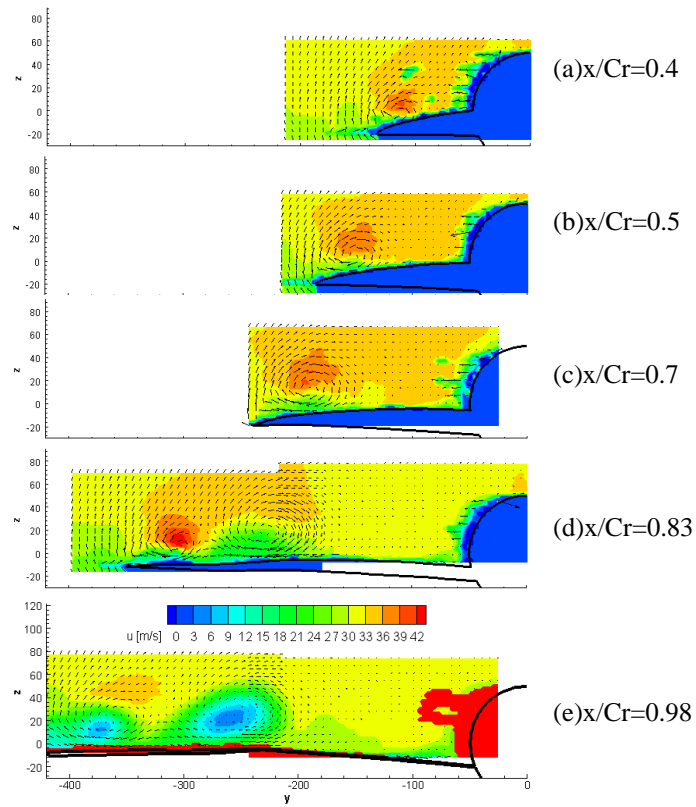


Fig.4 Averaged velocity vectors and streamwise velocity contours at several chordwise locations (Baseline Configuration, $\alpha=12^\circ$)

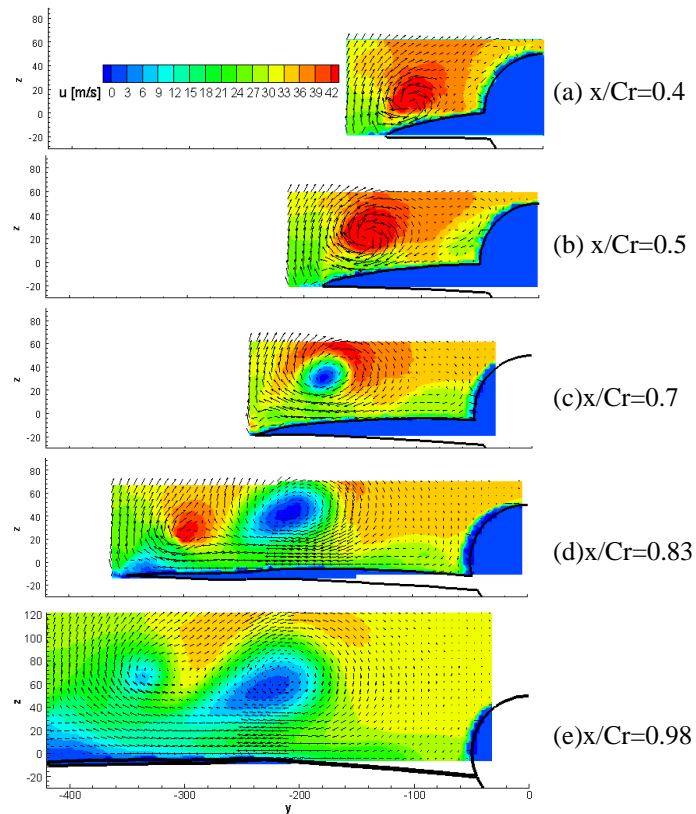


Fig. 5 Averaged velocity vectors and streamwise velocity contour at several chordwise locations (Baseline Configuration, $\alpha=20^\circ$)

VORTEX BEHAVIORS OVER A CRANKED ARROW WING CONFIGURATION AT HIGH ANGLES OF ATTACK

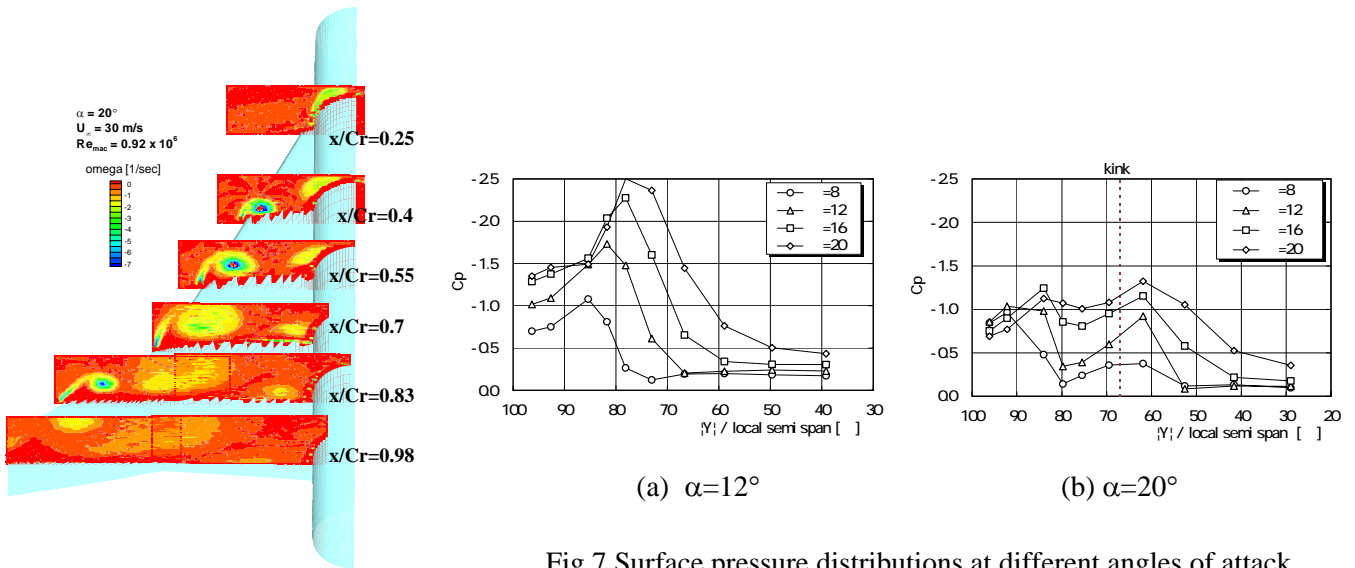


Fig.7 Surface pressure distributions at different angles of attack

Fig. 6 x-direction vorticity (ω) distributions at several chordwise locations ($\alpha=20^\circ$)

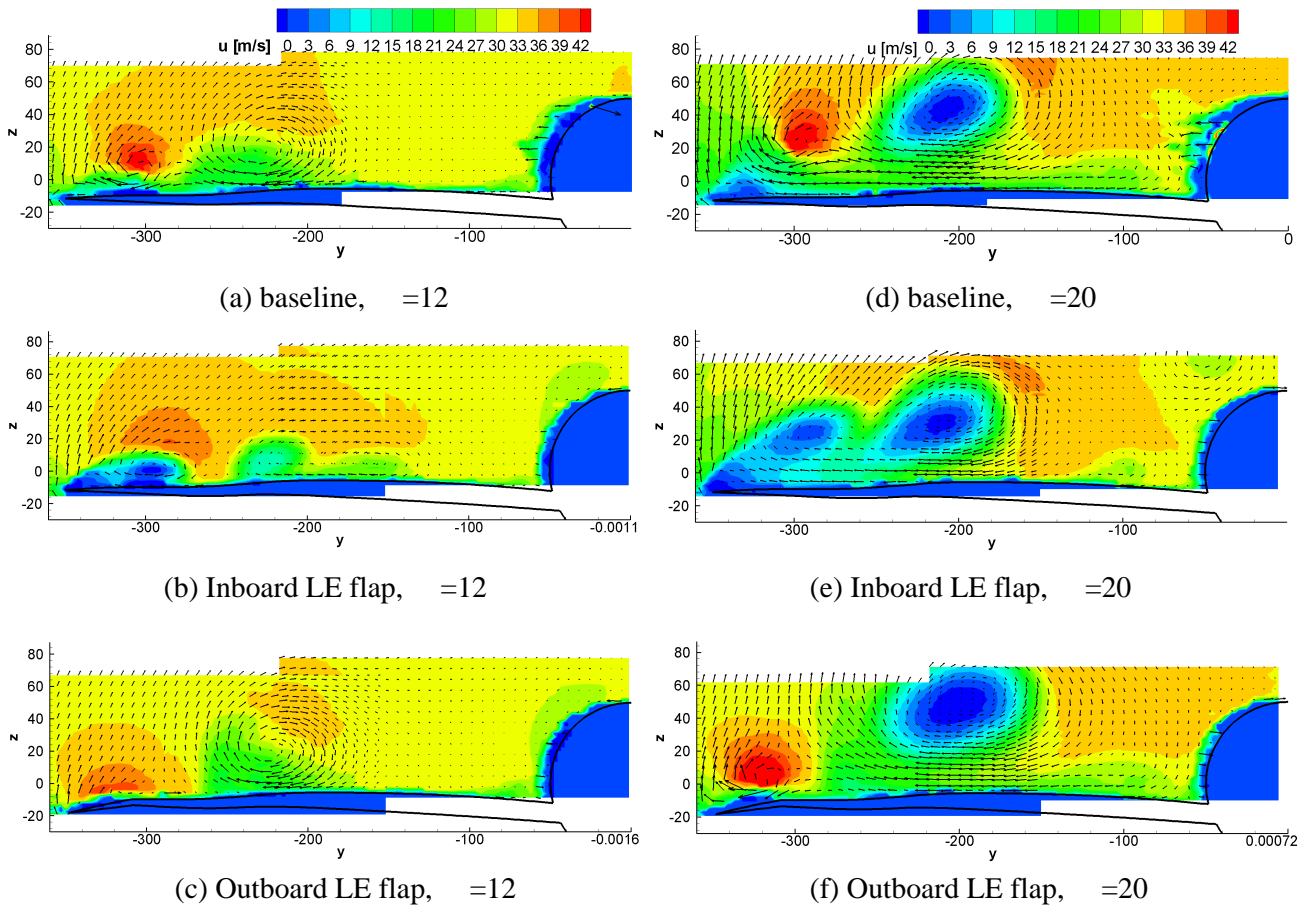


Fig.8 Averaged velocity vectors and streamwise velocity contours on models with different flap deflections ($x/Cr=0.83$)

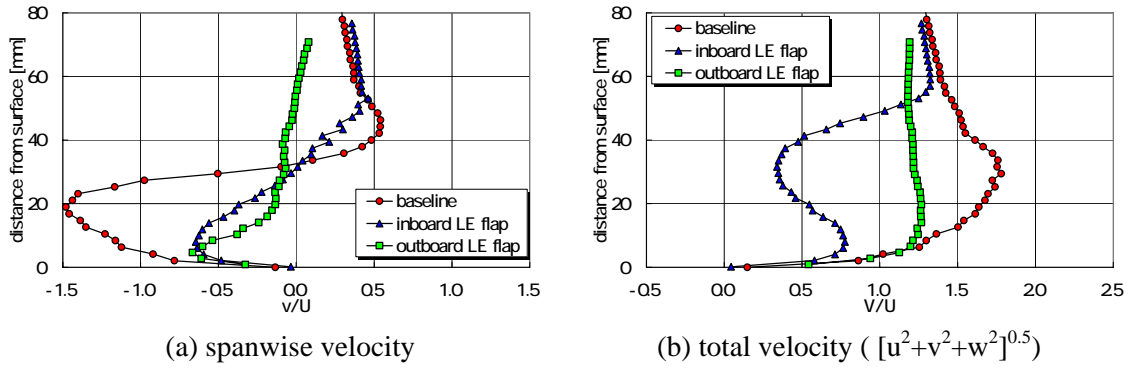


Fig.9 Velocity distribution at $y=-300\text{mm}$ ($\alpha=20^\circ$, $x/Cr=0.83$)

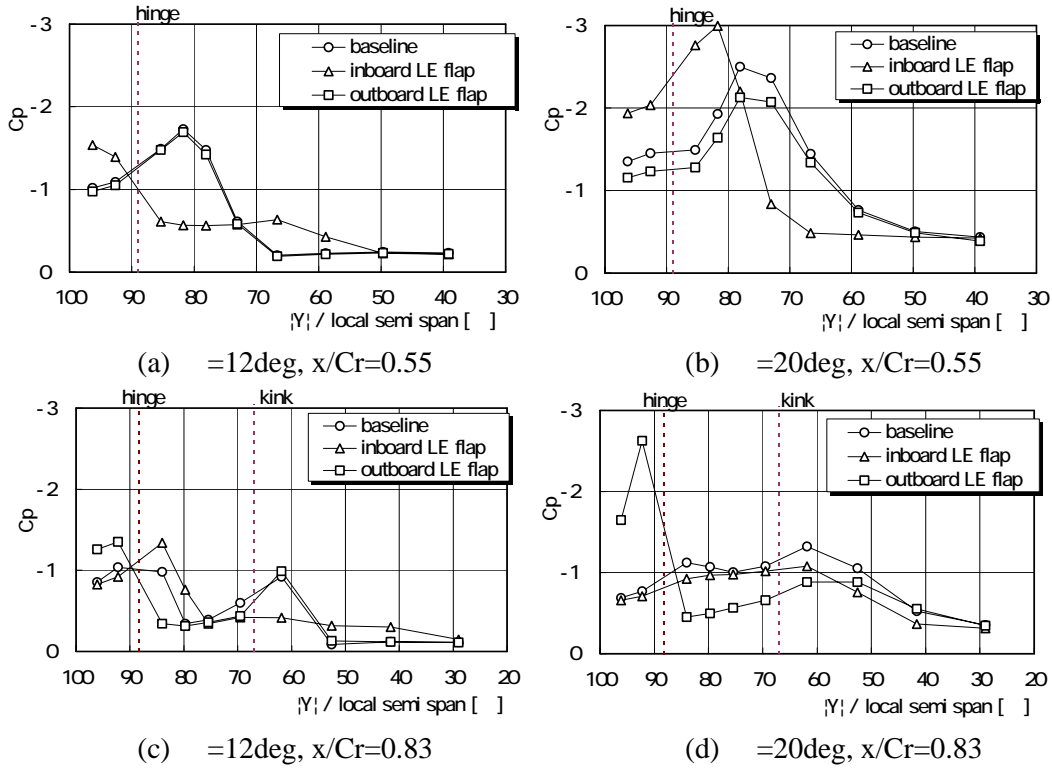


Fig.10 Surface pressure distributions on models with different flap deflections